JOURNAL OF AIRCRAFT
Vol. 41, No. 4, July–August 2004

Simulations of Store Separation from an F/A-18 with a Cartesian Method

Scott M. Murman*
ELORET, Moffett Field, California 94035
Michael J. Aftosmis†
NASA Ames Research Center, Moffett Field, California 94035
and
Marsha J. Berger‡
Courant Institute New York, New York 10012

Coupled computational fluid dynamics with six-degree-of-freedom trajectory predictions using an automated Cartesian method are demonstrated by simulating a GBU-31/Joint Direct Attack Munition store separating from an F/A-18C aircraft. Numerical simulations are performed at two Mach numbers near the sonic speed and compared with flight-test telemetry and photographic-derived data. For both Mach numbers, simulation results using a sequential-static series of flow solutions are contrasted with results using a time-dependent approach. Both numerical approaches show good agreement with the flight-test data through the first 0.25 s of the trajectory. At later times the sequential-static and time-dependent methods diverge, after the store produces peak angular rates; however, both remain close to the flight-test trajectory.

Nomenclature

C_A	=	axial-force coefficient
C_l	=	rolling-moment coefficient
C_m	=	pitching-moment coefficient
C_N	=	normal-force coefficient
C_n	=	yawing-moment coefficient
C_Y	=	lateral-force coefficient
h	=	altitude
I	=	moment of inertia
L	=	length
M	=	Mach number
S	=	area
t	=	time
α	=	angle of attack, deg
γ	=	dive angle, deg

Subscripts

ref	=	reference quantity
x, y, z	=	Cartesian directions
∞	=	freestream

I. Introduction

TRAJECTORY prediction is an important element in computational-fluid-dynamics (CFD) simulations of bodies undergoing unconstrained, or partially constrained motion. Modeling this behavior involves integrating the Newton–Euler equations for six-degree-of-freedom (6-DOF) rigid-body motion, in response to aerodynamic and other externally applied loads. Numerous important applications for such models exist, including store separation from an aircraft, booster separation from a space launch vehicle, canopy or shroud separation, and simulation of flight-control systems. Many CFD technologies have been demonstrated for 6-DOF simulations, including structured overset,[1,2] unstructured tetrahedral,[3,4] and hybrid prismatic/Cartesian.[5] The current work demonstrates an integrated package for performing 6-DOF simulations coupled with an inviscid, Cartesian embedded-boundary method.

Such non-body-fitted, Cartesian methods are particularly interesting for 6-DOF applications because they can be made both extremely fast and robust and the volume meshing can proceed automatically. Moreover, they are comparatively insensitive to the complexity of the input geometry because the surface description is decoupled from the volume mesh. In the current work, the "cut-cell" Cartesian meshing scheme of Aftosmis et al.[6] is utilized. The intersection of the solid geometry with the regular Cartesian hexahedra is computed, and polyhedral cells that contain the embedded boundary are formed. This volume meshing procedure is robust, computationally efficient, and does not require user intervention.

To demonstrate the utility of the Cartesian 6-DOF package, a U.S. Navy GBU-31 Joint Direct Attack Munition (JDAM) store (compare Fig. 1) separating from an F/A-18C is simulated using both sequential-static and time-dependent methods. This transonic JDAM separation was put forward by the Navy as a "challenge" to the CFD community because it exhibited behavior that could not reliably be predicted with conventional store separation analysis tools (compare Cenko[7] and Cenko et al.[8]). The JDAM separation provides an attractive demonstration case because it contains a complex aircraft geometry, flight telemetry, and photographic-derived quantitative data, and also because it has been simulated by numerous other CFD methods.[9–15] These previous CFD simulations can be broken into two broad classes: those which computed a set of static solutions that were used with a store trajectory simulation package and those which computed the trajectory of the store within the CFD simulation process. Both of these approaches are supported with the current methods, and a cost comparison will be presented.

The discussion begins by reviewing the geometry used in the simulations and briefly outlines the numerical scheme. Next it presents computed results for the JDAM separation flight conditions just below and just above sonic speed ($M_\infty = 0.962$ and 1.055). These results are directly compared to both flight telemetry and photographic-derived data. The computational cost for the current method is provided, along with a summary of the current results

Presented as Paper 2003-1246 at the AIAA 41st Aerospace Sciences Meeting and Exhibit, Reno, NV, 06 January 2003; received 13 January 2003; revision received 30 May 2003; accepted for publication 1 June 2003.

*Senior Research Scientist; smurman@nas.nasa.gov. Member AIAA.
†Research Scientist, MS T27B. Senior Member AIAA.
‡Professor, 251 Mercer Street. Member AIAA.

Fig. 1 U. S. Navy GBU-31 Joint Direct Attack Munition (JDAM).

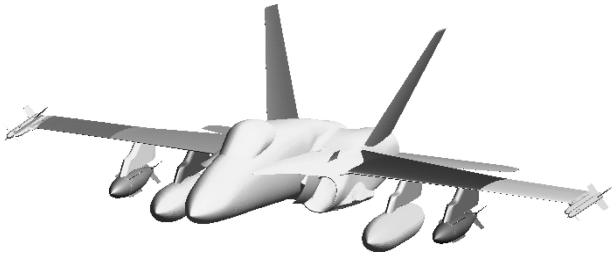

Fig. 2 F/A-18C surface geometry.

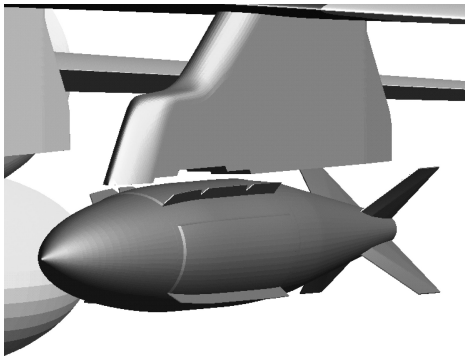

Fig. 3 Close-up view of triangulated JDAM beneath wing pylon.

and topics for future work. A detailed description and verification of the stand-alone 6-DOF package used with the current scheme is included in Ref. 16.

II. Numerical Scheme

A. Geometry and Computational Mesh

The surface geometry was provided as a set of structured surface patches. These were converted to water-tight surface triangulations of the various components. The addition of an internal duct connecting the engine diffuser face to the exit nozzle was required in order to form a water-tight fuselage. The component geometry for the complete F/A- 18C is shown in Fig. 2, with water-tight components shown with different colors. All of the major components of the geometry are modeled, including the empennage, AIM-9 wing-tip missile and rail, wing with leading-edge extensions (LEX), the LEX fence, the engine inlet including boundary-layer vents, and the wing pylons holding a 330-gal external fuel tank (EFT) inboard and the GBU-31 JDAM outboard. Note that the flight configuration did not contain the AIM-9 wing-tip missiles. Figure 3 shows a closeup view of the JDAM in its initial position beneath the port, outboard wing pylon. The attachment hardware and ejector mechanism is not modeled.

Using the automated Cartesian meshing scheme of Aftosmis et al.,[6] the triangulated surface was used to generate an unstructured Cartesian volume mesh by subdividing the computational domain based upon the geometry. The sharp geometric features contain refined cells, whereas areas away from the geometry maintain a relatively coarse spacing. The intersection of the solid geometry with the regular Cartesian hexahedra is computed, and polyhedral cells that contain the embedded boundary are formed. Regions interior to the solid geometry are removed. The solid-wall boundary conditions for the flow solver are then specified within these cut-cell polyhedra.

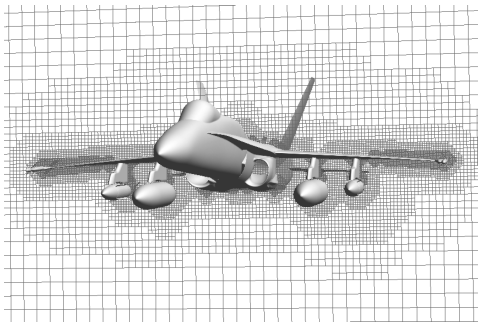

Fig. 4 Cutting plane through the Cartesian volume mesh.

In addition to mesh refinement near geometric features, prespecified adaption regions are arranged around the major components of the F/A-18 aircraft to resolve the shock structures that occur at the current flow conditions. The adaption region that surrounds the JDAM translates with the center of mass (c.m.) location as the store drops. In the future, these prespecified regions will be replaced with automated solution and geometry adaptation similar to the steady-state scheme outlined by Aftosmis and Berger.[17] A mesh refinement comparison was performed for the static, steady-state simulation with the JDAM in its initial position at the Mach 0.962 flight conditions (compare Table 1). The resulting volume mesh is isotropic and contains 3.8 million cells with a surface resolution of 1.0 in. A volume mesh cutting plane through the wing is shown in Fig. 4. Details of the mesh adaptation to the moving geometry will be presented in Sec. III.

B. Flow Solver

The inviscid, parallel multigrid flow solver of Aftosmis et al.[18] provides static, steady-state flow simulations for Cartesian meshes. Recently, this flow solver has been extended to provide capability for time-dependent flows, including dynamic simulations with rigid bodies in relative motion.[19,20] The current work implements an independent 6-DOF module, which can be utilized as a stand-alone external application, or tightly coupled within the time-dependent flow solver. A flow diagram for the 6-DOF/CFD simulation process is shown in Fig. 5. The geometry manipulation protocol (GMP) is utilized to integrate the independent mesh generation, flow solver, postprocessing, and 6-DOF steps into a unified computational framework.

Table 1 Computed flight conditions

Parameter	Case 1	Case 2
Mach number M_∞	0.962	1.055
Altitude h, ft	6332	10,832
AOA α, deg	0.46	−0.65
Dive angle γ, deg	43.0	44.0

Table 2 Original modeled F/A-18C/GBU-31 ejector forces (compare Refs. 7 and 13)

Time, s	Forward ejector force, lbf	Aft ejector force, lbf
0.00	97	97
0.01	206	223
0.02	531	283
0.03	1053	549
0.04	4723	988
0.05	4641	4708
0.06	4542	4633
0.07	4414	4528
0.08	4255	4386
0.09	0	4243
0.10	0	0

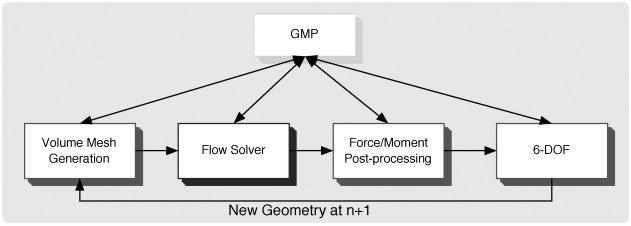

Fig. 5 Process diagram for 6-DOF simulations.

The 6-DOF module decomposes the rigid-body motion into a translation of the center of mass and a rotation about an axis passing through the c.m. location. The position of the c.m. is updated using Newton's laws of motion in the inertial frame, whereas the rotation of the body is determined by numerically integrating Euler's equations of motion in a body principal-axis system. The rotational position of the body is specified using Euler parameters, which are updated by numerical integration of the angular velocity. General external applied forces, in either the aerodynamic or body coordinate frames, can be specified. A detailed discussion of the 6-DOF model, along with validation test cases is presented in Ref. 16.

C. Ejector Force Model

The JDAM is forced away from its wing pylon by means of identical piston ejectors located in the lateral plane of the store, 10.11 in. forward of the c.m., and 9.89 in. aft. The ejectors extend during operation for 6 in., and the force of each ejector is a polynomial function of this stroke extension (compare Cenko[7]). As the store moves away from the pylon, it begins to pitch and yaw as a result of aerodynamic forces, and the stroke length of the individual ejectors responds asymmetrically. This response of the ejectors to the store motion is modeled, and the result is presented as a function of time for each piston. This modeling process for the F/A-18/JDAM is described by Fortin et al.,[13] and the results are presented in Table 2. A consistent theme with previous simulations is that this ejector model is limited (see Cenko et al.[8]). Because even slight errors in the initial trajectory of the store can become augmented as the separation simulation is marched forward in time, researchers have modified either the ejector model[8,14] or the computed JDAM trajectory[13] in order to provide a realistic store separation. Physically, the JDAM is constrained by the ejector mechanism, which is not accounted for in simplistic models. For example, the JDAM cannot be allowed to pitch nose down without bound, as physically the aft ejector would restrict such motions.

Although the focus of the current work is not to develop an ejector model for the F/A-18/JDAM configuration, simulating the store separation with an ejector model that has known inaccuracies serves little purpose. An attempt to modify the ejector model to account for the constraint imposed by the wing pylon and ejector mechanism is proposed. First, following the a posteriori observations of Cenko et al.[8] the magnitude of the ejector forces was increased by 25%. Next, it is assumed that while the ejectors are accelerating (roughly $0.0 < t < 0.05$ s) the rotation of the JDAM is restricted by friction between the ejector pistons and the JDAM surface. From examining the flight data, it is clear that the rotation is not completely restrained, so that a friction resistance equivalent to 50% of the aerodynamic moments is imposed initially, which is allowed to linearly decrease to no resistance at $t = 0.05$ s. The modified ejector forces and friction resistance are used with all of the simulation results presented here.

III. Computed Results

The numerical scheme outlined in the preceding section was used to compute the separation of a GBU-31/JDAM from an F/A-18C at the two flight conditions listed in Table 1. The inertial properties for the JDAM were provided by the Navy and are summarized in Table 3. The pylon ejector modeling was discussed in Sec. II.C. This configuration was tested in the wind-tunnel using a captive trajectory system and in flight by the U.S. Navy (see Cenko[7]). Near sonic speeds, the variation of pitching and yawing moments experienced by the JDAM with Mach number becomes highly nonlinear. This strong nonlinearity makes trajectory prediction using linearized methods (see Keen[22]) challenging. High-fidelity CFD methods can potentially provide a cost-effective, accurate tool for predicting store trajectories at all flight conditions.

Full-aircraft static, steady-state simulations were computed with the JDAM in its initial position below the wing pylon for both flight conditions. Surface-pressure contours on the body surface are shown in Fig. 6 for the $M_\infty = 1.055$ simulation. The shock reflections on

Table 3 GBU-31 JDAM inertial properties and reference quantities from Cenko[7]

Parameter	Value
S_{ref}	1.767 ft^3
L_{ref}	1.5 ft
c.m.	62.66 in. from nose
Mass	2059.44 lbm
I_{xx}	20.02 slug-ft^2
I_{yy}	406.56 slug-ft^2
I_{zz}	406.59 slug-ft^2
I_{xz}	−0.680 slug-ft^2
I_{xy}	0.860 slug-ft^2
I_{yz}	0.00 slug-ft^2

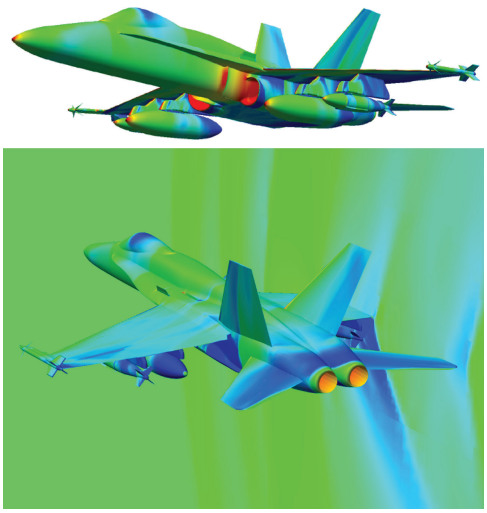

Fig. 6 Surface-pressure contours on the F/A-18 surface.

the wing pylons caused by the stores are visible, as are the shocks that appear on the canopy, wing, and empennage. The cutting plane shows the resolution of the shocks to the far field.

The computed forces and moments on the JDAM from the initial static simulations are compared with wind-tunnel and flight data in Table 4. No uncertainty predictions or error estimates are available for the wind-tunnel or flight data. The computed results are in good agreement with the flight and tunnel data, with the largest discrepancy occurring in yawing moment at $M_\infty = 0.962$, which is less than 10% variation. In general, the computed results compare more favorably to the flight data at $M_\infty = 1.055$ than 0.962, as would intuitively be expected.

A. Sequential-Static Simulations

The current work simulates the separation of the JDAM using both time-dependent and steady-state methods. The inertia of the GBU-31 is very large, and the expectation is that unsteady effects are minimal, at least while the store is still close to the pylon. This thesis is examined by comparison of time-dependent separation results with sequential-static simulations. The sequential-static results are presented first. In this method, the store is repositioned at the new time level based upon the computed loads at the previous time level (compare Fig. 5, Sec. II.B); however, the flow solver ignores the motion of the body and treats it as a static, steady-state problem at the new body position. This approach can be attractive when accurate, time-dependent, moving-body flow solvers are not available. A common technique with captive store trajectory systems is to modify the angle of attack of the store to account for the plunge velocity. A similar technique could easily be integrated with the sequential-static simulation; however, the current computations do not use this correction. In the current work, the computed solution at the previous time level is transfered to the new mesh, after the body has been repositioned, to use as an initial guess. This transfer process, which is described in Ref. 20 for the time-dependent scheme, minimizes the computational cost because the solution at the previous time level provides a good initial guess for the solution at the next time level.

Table 4 Computed forces and moments on the JDAM for the initial store position (Wind-tunnel and flight data taken from Cenko[7])

Data source	C_A	C_Y	C_N	C_l	C_m	C_n
	$M_\infty = 0.962$, $\alpha = 0.46$ *deg*, $\gamma = 43$ *deg*					
Wind tunnel	——	0.31	0.11	——	−2.32	−2.76
Flight	——	0.31	0.15	——	−2.5	−2.8
Computed	0.67	0.33	0.09	0.16	−2.36	−2.49
	$M_\infty = 1.055$, $\alpha = -0.65$ *deg*, $\gamma = 44$ *deg*					
Wind tunnel	——	0.24	−0.02	——	−2.07	−2.56
Flight	——	0.25	−0.05	——	−2.0	−2.2
Computed	0.65	0.28	−0.03	0.15	−2.02	−2.11

A constant time step of $\Delta t = 0.0075$ s. is used for these simulations. Because of time constraints, it was not possible to perform a time-resolution study for these cases. Information travels roughly one JDAM body length in 12 time steps using this resolution, which is felt to be reasonable. All simulations were run through $t = 0.45$ s.

Computed results for the relative displacement of the JDAM c.m. location are compared to flight data for both computed cases in Fig. 7. Similar plots for the angular position and angular velocity of the JDAM are shown in Figs. 8 and 9, respectively. Below $t = 0.20$ s. the predicted displacement and angular position are in

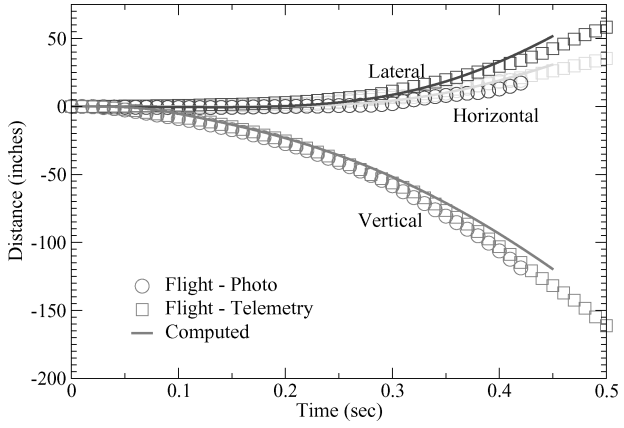

a) $M_\infty = 0.962$, $\alpha = 0.046$ deg, $\gamma = 43$ deg

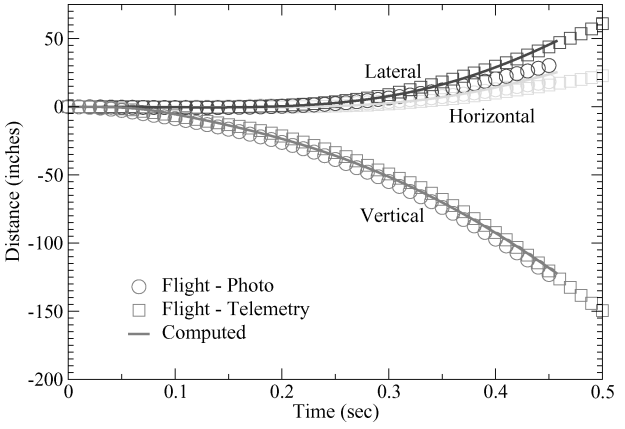

b) $M_\infty = 1.055$, $\alpha = -0.065$ deg, $\gamma = 44$ deg

Fig. 7 Relative displacement for sequential-static simulations.

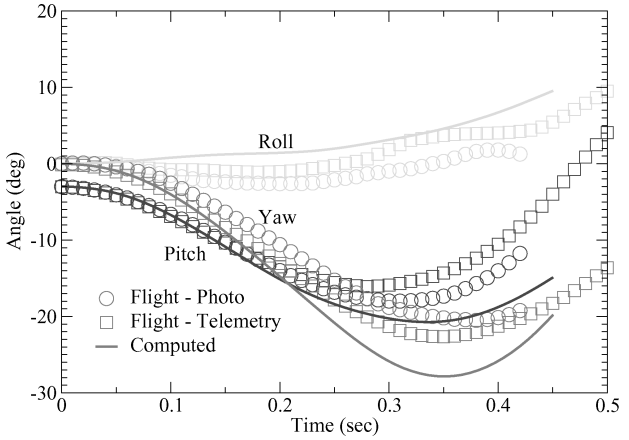

a) $M_\infty = 0.962$, $\alpha = 0.046$ deg, $\gamma = 43$ deg

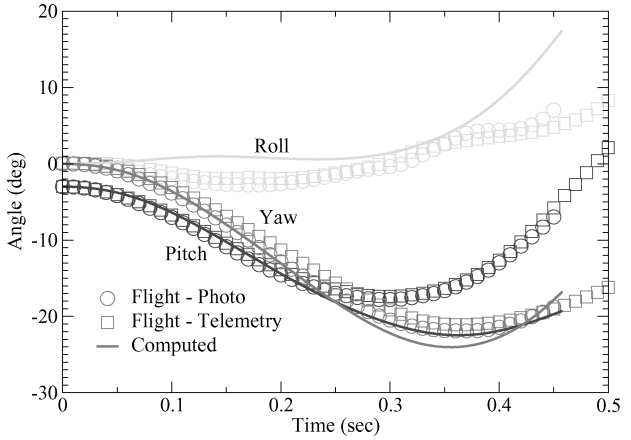

b) $M_\infty = 1.055$, $\alpha = -0.065$ deg, $\gamma = 44$ deg

Fig. 8 Angular positions for sequential-static simulations.

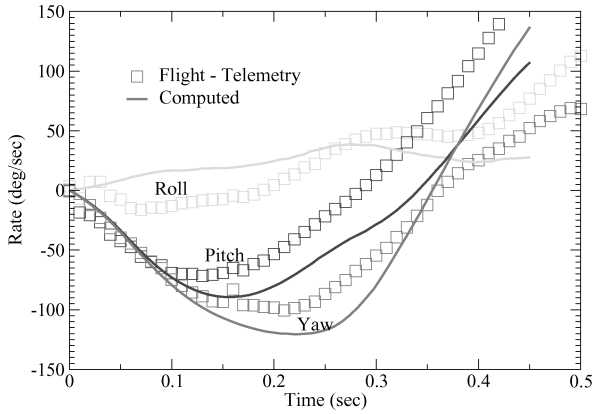

a) $M_\infty = 0.962$, $\alpha = 0.046$ deg, $\gamma = 43$ deg

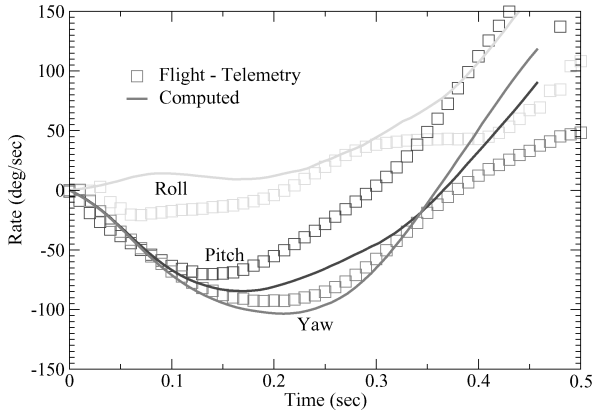

b) $M_\infty = 1.055$, $\alpha = -0.065$ deg, $\gamma = 44$ deg

Fig. 9 Angular rates for sequential-static simulations.

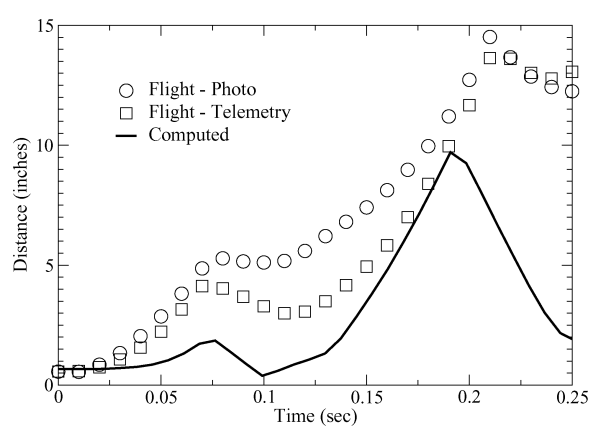

a) $M_\infty = 0.962$, $\alpha = 0.046$ deg, $\gamma = 43$ deg

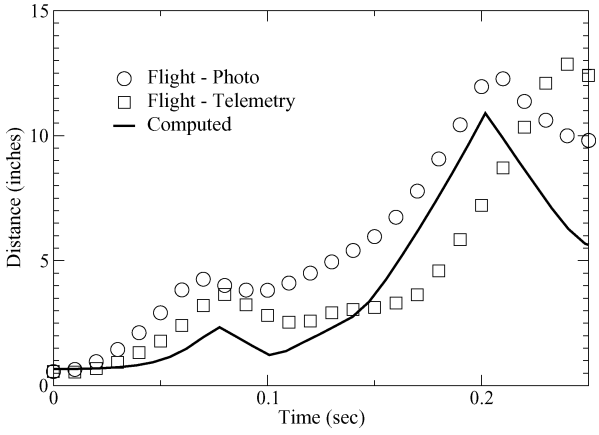

b) $M_\infty = 1.055$, $\alpha = -0.065$ deg, $\gamma = 44$ deg

Fig. 10 Miss distances for sequential-static simulations.

good agreement with the flight data; however, the angular rate prediction has begun to degrade. At later times, the cumulative errors in angular position lead to a poorer agreement with the flight data, while the predicted displacement of the c.m. correlates well through the simulation. The accuracy of the current predictions is commensurate with previous computed results for this same configuration.[9–15] These earlier computed results contain several viscous simulations. The degradation of the predicted angular orientation will be discussed in the next section with the time-dependent simulations results.

The miss distance, or the distance between the closest points on the JDAM and any other component of the aircraft, is presented in Fig. 10. Although the predicted displacement and angular position are in good agreement with the flight data over the time interval presented, the miss distance underpredicts the separation between the store and the wing pylon. The explanation for this is that as the ejectors push away the store there is a reaction force applied to the pylon. This reaction leads to a rolling moment on the aircraft, which rolls the pylon away from the JDAM, that is, increases the miss distance between the two. This reaction of the aircraft is not modeled in the current work (or in previous work in the literature), and hence the separation is underpredicted. The closest miss, which occurs near $t = 0.10$ s, is caused by the tail fins sweeping under the pylon as the JDAM yaws nose outboard. At $t = 0.20$ s the closest component changes from the pylon to the EFT, as the body continues to yaw and fall.

Figure 11 shows a series of snapshots of the surface pressure as the JDAM falls through $t = 0.30$ s in the $M_\infty = 1.055$ simulation. The nose of the store is forced downward and outboard by the shock from the leading edge of the wing. This causes the JDAM to pitch and yaw immediately upon release from the holding pylon. The change in shock structure on the pylon as the JDAM releases can be seen, as well as changes on the aft portion of the aircraft fuselage. As the JDAM falls, the tail fins provide restoring moments, which cause the store pitch back nose up and inboard (compare with Figs. 8 and 9). A complementary series of snapshots, which show the adaptation of the mesh to the moving geometry, are shown in Fig. 12. The mesh automatically adapts to the new geometry position and also coarsens in regions the body has moved through.

B. Time-Dependent Simulations

The preceding section presented results of coupled 6-DOF/CFD trajectory predictions using sequential-static flow simulations. This is contrasted here with fully coupled, time-dependent trajectory simulations performed using the Cartesian moving-body solver described in Ref. 20. Analyzing Fig. 9, the angular rate prediction for the sequential-static simulations begins to degrade after the rotation of the body experiences both the highest velocities and an inflection point in the acceleration, that is, near $t = 0.125$ for pitch rate and $t = 0.20$ for yaw rate. This combination of high velocity and change in sign of acceleration indicates regions in the store trajectory where dynamic, or unsteady effects, can be significant. This is examined in Figs. 13–16, which present relative displacement, angular orientation, angular rate, and miss distance for the time-dependent simulations, compared with the sequential-static simulations and flight-test data. The data shows that the two CFD trajectory simulations are in good agreement prior to $t = 0.125$, when the pitch rate reaches a maximum. After this point, the predicted pitch behavior is improved; however, the yaw prediction degrades. The pitch and yaw trajectories are similar in the sequential-static and time-dependent simulations, except for the response near the maximum rates, that is, the dynamic effects are largely localized to

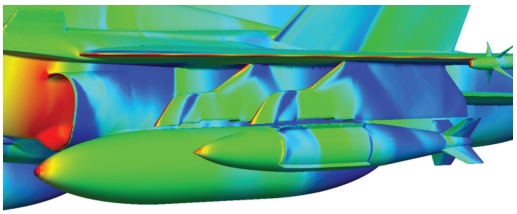

a) $t = 0.0$ s.

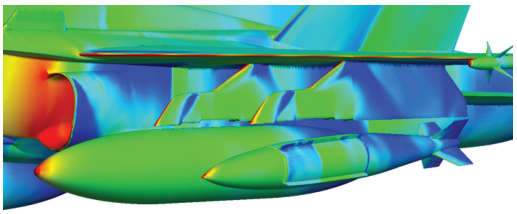

b) $t = 0.1$ s.

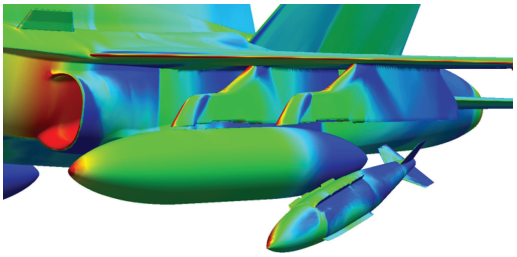

c) $t = 0.2$ s.

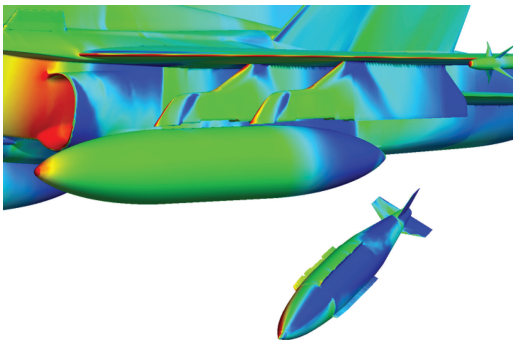

d) $t = 0.3$ s.

Fig. 11 Surface pressure contours during JDAM separation.

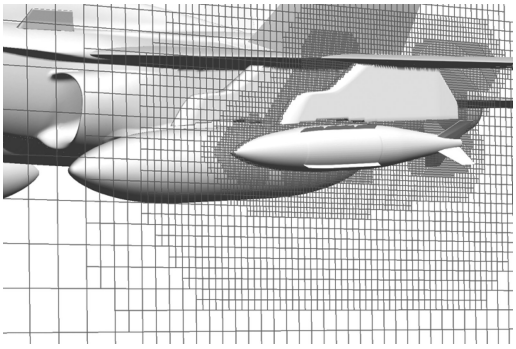

a) $t = 0.0$ s.

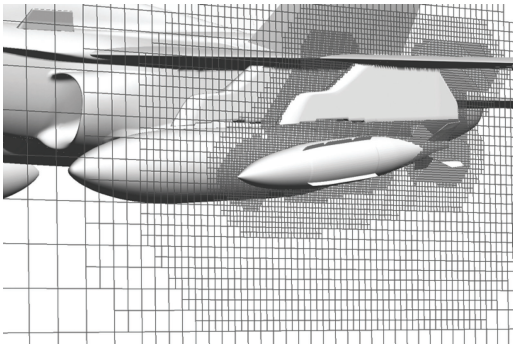

b) $t = 0.1$ s.

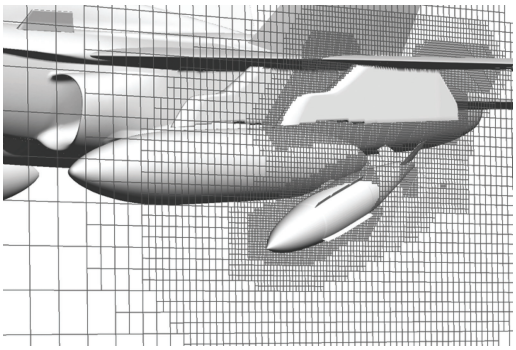

c) $t = 0.2$ s.

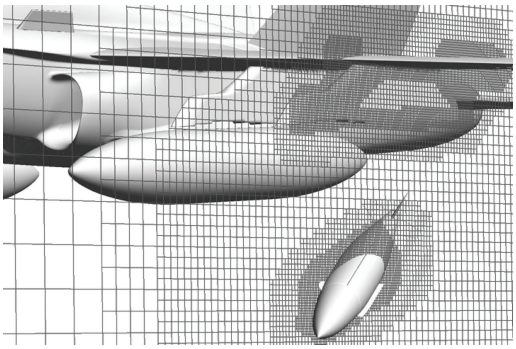

d) $t = 0.3$ s.

Fig. 12 Cutting planes through the volume mesh during JDAM separation.

this region of the trajectory. The relative displacement prediction is nearly unchanged in the time-dependent simulations at $M_\infty = 1.055$; however, $M_\infty = 0.962$ shows a relatively significant change in vertical drop, which is not currently well understood. The underprediction of the separation distance after $t = 0.20$ is caused by the overpredicted yaw angle in both the sequential-static and time-dependent simulations, which causes the tail fins to remain close to the EFT.

Consistently, in both the sequential-static and time-dependent simulations, the predicted roll behavior of the JDAM does not correlate well with the flight data. This is not unique to the current work and has been noted in previous trajectory predictions for this configuration.[7–15] Cenko[7] notes "[roll attitude] is the hardest to predict, fortunately has a minimal impact on the trajectory." Although it is true that small changes in roll orientation are likely insignificant, the current predictions consistently vary from the flight data by roughly 5 deg of roll, and even while the store is still being pushed by the ejectors the roll is predicted in the opposite direction. Because the roll orientation can affect the restoring moment provided by the tail fins, it is unclear whether these small differences can accumulate to produce the larger errors seen in pitch and yaw prediction in the current work.

C. Computational Cost

The computational cost for the current Cartesian/6-DOF scheme is presented in two forms; absolute and relative to computing a fixed database of static results. Note that the current work was performed with tools designed for computing a single fixed static simulation, and little effort has gone into tailoring them for sequential moving-body calculations. All simulated results presented here were computed using NASA Ames' 1024 CPU, single-image SGI Origin 3000

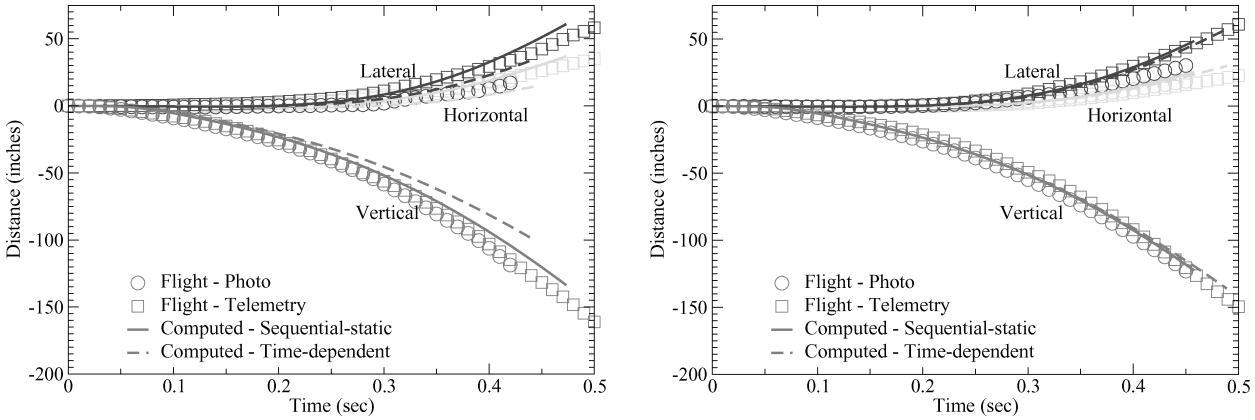

a) $M_\infty = 0.962$, $\alpha = 0.046$ deg, $\gamma = 43$ deg **b)** $M_\infty = 1.055$, $\alpha = -0.065$ deg, $\gamma = 44$ deg

Fig. 13 Relative displacement for time-dependent simulations.

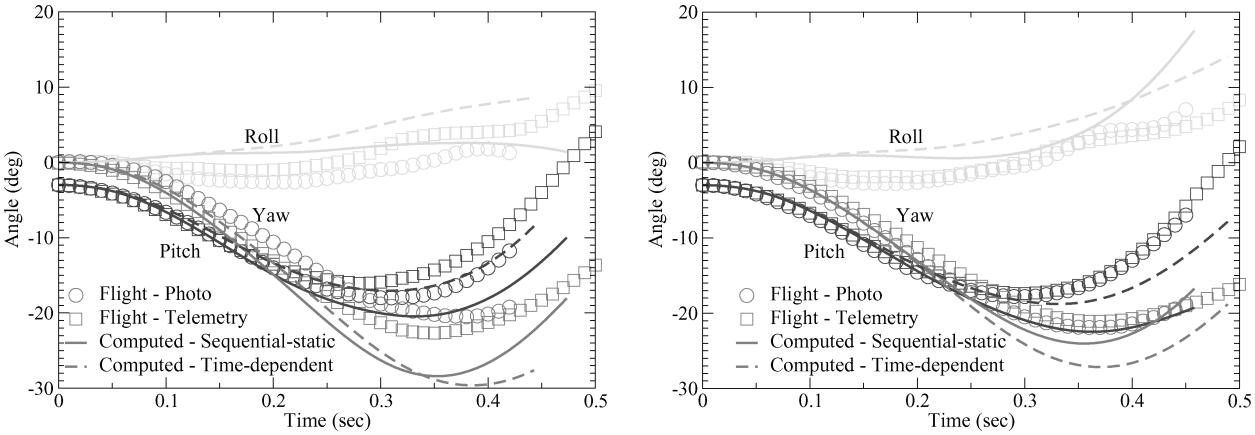

a) $M_\infty = 0.962$, $\alpha = 0.046$ deg, $\gamma = 43$ deg **b)** $M_\infty = 1.055$, $\alpha = -0.065$ deg, $\gamma = 44$ deg

Fig. 14 Angular positions for time-dependent simulations.

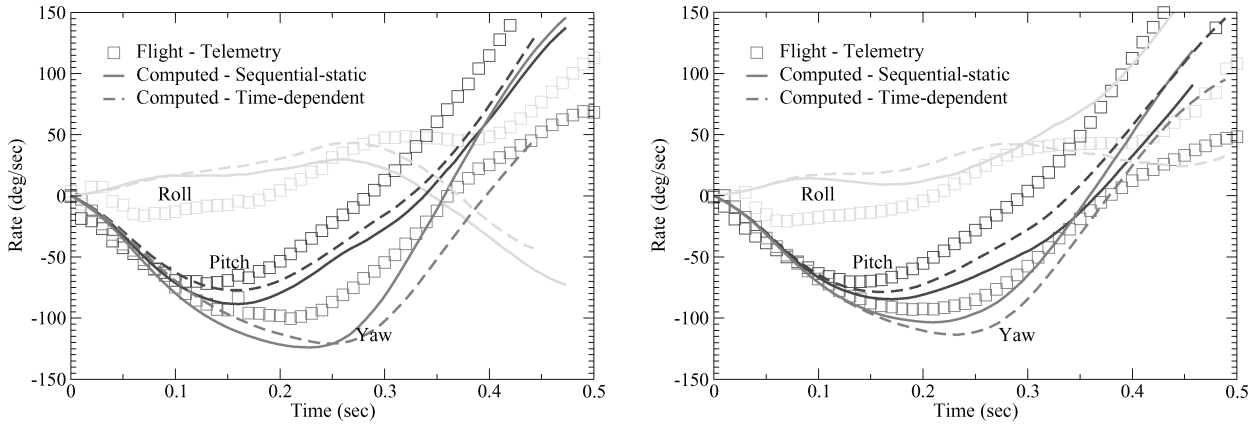

a) $M_\infty = 0.962$, $\alpha = 0.046$ deg, $\gamma = 43$ deg **b)** $M_\infty = 1.055$, $\alpha = -0.065$ deg, $\gamma = 44$ deg

Fig. 15 Angular rates for time-dependent simulations.

(O3K), which has 600-MHz MIPS4 processors. The current flow solver has been demonstrated to scale linearly to 512 CPUs on this architecture for problems of the size considered here. The current simulations all required roughly 260 single CPU hours of computational time to complete 60 time steps, with less than 5% of the computational time utilized by the volume mesh generation process. The sequential-static and time-dependent simulations require the same computational time with the current scheme. The wall-clock time to complete a simulation using 32 CPUs is approximately 15 hours. This time reflects the adverse effects of the serial mesh generation on the parallel efficiency of the entire process. Parallelizing the entire process, including volume mesh generation, will be a major focus of future work.

The current work couples together the CFD flow solver and the 6-DOF trajectory prediction. Another method of integrating high-fidelity CFD with 6-DOF predictions is to build a computational

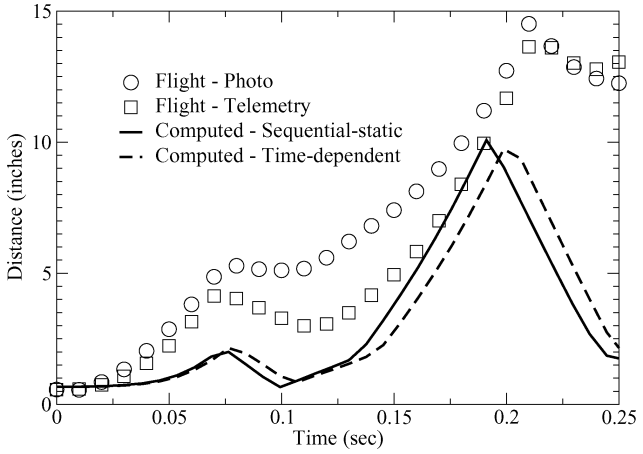

a) $M_\infty = 0.962$, $\alpha = 0.046$ deg, $\gamma = 43$ deg

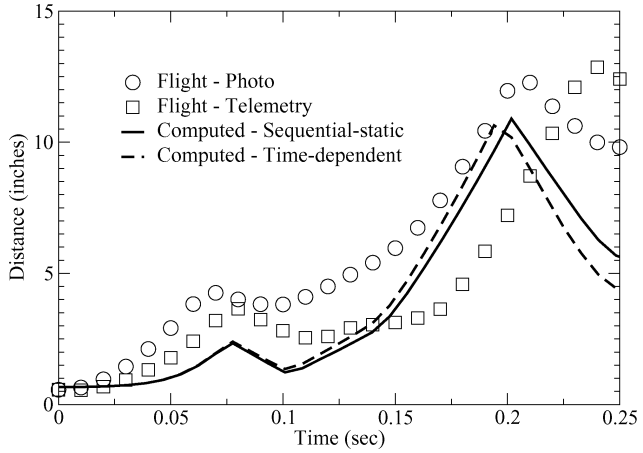

b) $M_\infty = 1.055$, $\alpha = -0.065$ deg, $\gamma = 44$ deg

Fig. 16 Miss distances for time-dependent simulations.

database of results and then "fly" 6-DOF trajectories through this computed database. The advantage of this approach is that once the initial database is created many 6-DOF trajectories can be computed essentially at no cost. The disadvantage of the database approach for 6-DOF simulations is the large number of computational cases required to build even a minimal database. For a single fixed wind vector (M_∞, α, β) there are six free parameters (three displacement and three angular position) for a static CFD database. ("Static" here refers to the absence of any dynamic stability derivative information.) If each of these is allowed to vary over 10 distinct states (which is relatively coarse), then 10^6 computed cases are required to fill the database. This is impractical even for wind-tunnel programs. It is possible to reduce the required independent variables by assuming that the horizontal and lateral relative displacements are much less than the vertical and that the roll orientation of the body can be ignored. This reduction leaves on the order of 1000 data points required for steady-state simulation.

In the current work, an initial steady-state calculation is required at the initial position of the store, and each time step costs roughly $\frac{1}{5}$ of a full static simulation. As 60 steps were required for a full simulation using the current timestep, the cost for the current coupled 6-DOF trajectory simulations is roughly 10 complete steady, static simulations. This implies that on the order of 100 such coupled simulations can be performed for the cost of building a coarse, approximate database. Further, each coupled simulation is independent, so that the simulations can be carried out in parallel. The higher accuracy and relatively low cost makes these coupled CFD/6-DOF simulations an attractive analysis tool.

IV. Summary

The utility of a coupled Cartesian/6-DOF trajectory prediction scheme has been demonstrated by simulation of a GBU-31 JDAM separating from an F/A-18C. The Cartesian scheme provides an automated, robust meshing scheme that can easily be integrated into a design analysis. The accuracy and computational cost of the current simulated results are commensurate with earlier results for the F/A-18C/JDAM separation computed using body-fitted approaches.

Future work will progress on two major fronts: understanding the discrepancies in predicted angular orientation that occur at later time levels and optimizing the flow simulation process for these moving-body simulations. There are many possible explanations, both computational and experimental, for the degradation in the predicted trajectory at later time levels. It is important to understand whether this behavior is related to the current approach so that it can be corrected, if necessary. The process optimization itself will mainly focus on parallelizing the volume mesh generation and incorporating solution-adaptive capability.

Acknowledgments

The authors would like to thank Alex Cenko of the U.S. Navy for his help in acquiring the geometry and Ralph Noack of the University of Alabama, Birmingham, for his assistance throughout this project. John Guse of Boeing generously supplied information regarding the inertial properties of the F/A-18C. Marsha Berger was supported in part by U.S. Air Force Office of Scientific Research Grant F19620-00-0099.

References

[1]Meakin, R. L., "Computations of the Unsteady Flow About a Generic Wing/Pylon/Finned-Store Configuration," AIAA Paper 92-4568-CP, Aug. 1992.

[2]Prewitt, N. C., Belk, D., and Shyy, W., "Multiple Body Trajectory Calculations Using the Beggar Code," AIAA Paper 99-0913, Jan. 1999.

[3]Löhner, R., and Baum, J. D., "Three-Dimensional Store Separation Using a Finite Element Solver and Adaptive Remeshing," AIAA Paper 91-0602, Jan. 1991.

[4]Cavallo, P. A., and Dash, S. M., "Aerodynamics of Multi-Body Separation Using Adaptive Unstructured Grids," AIAA Paper 2000-4407, Aug. 2000.

[5]Welterlen, T. J., and Leone, C., "Application of Viscous Cartesian CFD to Aircraft Store Carriage and Separation Simulation," AIAA Paper 96-2453, June 1996.

[6]Aftosmis, M. J., Berger, M. J., and Melton, J. E., "Robust and Efficient Cartesian Mesh Generation for Component-Based Geometry," AIAA Paper 97-0196, Jan. 1997; also *AIAA Journal*, Vol. 36, No. 6, 1998, pp. 952–960.

[7]Cenko, A., "F-18/JDAM CFD Challenge Wind Tunnel Flight Test Results," AIAA Paper 99-0120, Jan. 1999.

[8]Cenko, A., Lutton, M., and Tutty, M., "F/A-18/C/JDAM Applied Computational Fluid Dynamics Challenge II Results," AIAA Paper 2000-0795, Jan. 2000.

[9]Tomaro, R. F., Witzeman, F. C., and Strang, W. Z., "A Solution on the F-18C for Store Separation Simulation Using Cobalt_{60}," AIAA Paper 99-0122, Jan. 1999.

[10]Woodson, S. H., and Brunner, C. W. S., "Analysis of Unstructured CFD Codes for Accurate Prediction of Aircraft Store Trajectories," AIAA Paper 99-0123, Jan. 1999.

[11]Welterlen, T. J., "Store Release Simulation on the F/A-18C Using Splitflow," AIAA Paper 99-0124, Jan. 1999.

[12]Fairlie, B. D., and Caldeira, R. H., "Prediction of JDAM Separation Characteristics from the F/A-18C Aircraft," AIAA Paper 99-0126, Jan. 1999.

[13]Fortin, F., Benmeddour, A., and Jones, D. J., "Application of the Canadian Code to the F/A-18C JDAM Separation," AIAA Paper 99-0127, Jan. 1999.

[14]Noack, R. W., and Jolly, B., "Fully Time Accurate CFD Simulations of JDAM Separation from an F-18C Aircraft," AIAA Paper 2000-0794, Jan. 2000.

[15]Sickles, W. L., Denny, A. G., and Nichols, R. H., "Time-Accurate Predictions of the JDAM Separation from an F-18C Aircraft," AIAA Paper 2000-0796, Jan. 2000.

[16]Murman, S. M., Aftosmis, M. J., and Berger, M. J., "Simulations of 6-DOF Motion with a Cartesian Method," AIAA Paper 2003-1246, Jan. 2003.
[17]Aftosmis, M. J., and Berger, M. J., "Multilevel Error Estimation and Adaptive h-Refinement for Cartesian Meshes with Embedded Boundaries," AIAA Paper 2002-0863, June 2002.
[18]Aftosmis, M. J., Berger, M. J., and Adomavicius, G., "A Parallel Multilevel Method for Adaptively Refined Cartesian Grids with Embedded Boundaries," AIAA Paper 2000-0808, Jan. 2000.
[19]Murman, S. M., Aftosmis, M. J., and Berger, M. J., "Numerical Simulation of Rolling-Airframes Using a Multi-Level Cartesian Method," AIAA Paper 2002-2798, June 2002.
[20]Murman, S. M., Aftosmis, M. J., and Berger, M. J., "Implicit Approaches for Moving Boundaries in a 3-D Cartesian Method," AIAA Paper 2003-1119, Jan. 2003.
[21]Murman, S. M., Chan, W. M., Aftosmis, M. J., and Meakin, R. L., "An Interface for Specifying Rigid-Body Motion for CFD Applications," AIAA Paper 2003-1237, Jan. 2003.
[22]Keen, K. S., "New Approaches to Computational Aircraft/Store Weapons Integration," AIAA Paper 90-0274, Jan. 1990.